EAI Endorsed Transactions
on Wireless Spectrum
Research Article EAI.EU

Advanced High-order Hidden Bivariate Markov Model Based Spectrum Prediction

Zhiming Hong[1], Yanxiao Zhao[1,*], Yu Luo[1], Guodong Wang[1] and Lina Pu[1]

[1]Department of Electrical and Computer Engineering,

South Dakota School of Mines and Technology, Rapid City, SD 57701 USA.

Abstract

The majority of existing spectrum prediction models in Cognitive Radio Networks (CRNs) don't fully explore the hidden correlation among adjacent observations. In this paper, we first develop a novel prediction approach termed high-order hidden bivariate Markov model (H^2BMM) for a stationary CRN. The proposed H^2BMM leverages the advantages of both HBMM and high-order, which applies two dimensional parameters, i.e., hidden process and underlying process, to more accurately describe the channel behavior. In addition, the current channel state is predicted by observing multiple previous states. Afterwards, the mobility of secondary users is fully considered and we propose an advanced approach based on H^2BMM, termed Advanced H^2BMM, to accommodate a mobile CRN. Extensive simulations are conducted and results verify that the prediction accuracy is significantly improved using the proposed (H^2BMM. The Advanced H^2BMM is also evaluated with comparison to H^2BMM and results show considerable improvements of H^2BMM in a mobile environment.

Received on 7 December 2017; accepted on 9 December 2017; published on 12 December 2017

Keywords: cognitive radio network, spectrum prediction, high-order hidden bivariate Markov model.

Copyright © 2017 Zhiming Hong *et al.*, licensed to EAI. This is an open access article distributed under the terms of the Creative Commons Attribution license (http://creativecommons.org/licenses/by/3.0/), which permits unlimited use, distribution and reproduction in any medium so long as the original work is properly cited.

doi:10.4108/eai.12-12-2017.153466

1. Introduction

Cognitive Radio Networks (CRNs) are commonly perceived as a promising solution to the issue of spectrum scarcity. In CRNs, Primary Users (PUs) and Secondary Users (SUs) refer to the authorized and unauthorized users of allocated channels, respectively [1]. SUs are allowed to access channels opportunistically without harmful interferences to PUs [2]. To implement CRNs successfully, spectrum sensing is an essential process, in which SUs must obtain awareness about the spectrum usage to avoid destructive interferences to PUs [3].

A traditional CRN requires SUs to continually conduct a spectrum sensing process [4]. Specifically, time is divided into slots which consist of a small portion of sensing period, followed by a relative long period for data transmission. SUs conduct regular sensing and update the sensing result every time slot, which leads to high computational complexity [5]. To speed up the sensing process and save more time for transmission, spectrum prediction is a favorable technology. Spectrum prediction refers to the process of estimating the future channel occupancy status by analyzing sensing history [6]. With prediction, SUs are not required to sense the channel every time slot and hence the time for data transmission is prolonged.

A few spectrum prediction schemes have been proposed in the recent literature. Authors in [7] summarize several state-of-the-art spectrum prediction techniques and illustrate their applications. In [8] [9] [10], Markov related prediction algorithm has been improved from Hidden Markov Model (HMM) to high-order HMM and Hidden Bivariate Markov Model (HBMM). The standard HMM [8], also named the first-order HMM, solely depends on one immediately prior state and the correlation with other previous states is not fully explored. To improve the accuracy, a high-order HMM is proposed and evaluated in [9] where the current channel state depends on more than one prior states. In addition, studies discover that the geometric distribution characteristic of HMM is not suitable for describing channel behaviors, especially when bursty transmissions occur [11]. To better model the cognitive radio channel, hidden bivariate Markov model (HBMM)

*Corresponding author. Email: yanxiao.zhao@sdsmt.edu

is proposed and applied to spectrum prediction in [10]. The main idea of HBMM is to further divide a channel state into multiple sub-states, forming an underlying process, so that the channel sub-state dwell time follows a Phase distribution.

As mentioned above, HBMM and high-order HMM are proposed separately to improve the standard HMM from two perspectives. In our paper, we first consider a stationary CRN and propose a novel prediction approaches, termed High-order Hidden Bivariate Markov model (H^2BMM), by leveraging the advantages of both high-order and HBMM. H^2BMM is to apply two dimensional parameters, i.e., hidden process and underlying process, to more accurately describe the channel behavior. In a stationary CRN, individual stationary SUs conduct H^2BMM to complete the tasks of sensing and prediction. Afterwards, we extend H^2BMM to a mobile CRN since mobility is an inherent feature in a wireless environment. In a mobile CRN, when SUs move, it is difficult for an individual SU to analyze the activity patterns of PUs along with its moving path [12]. Therefore, the concept of cooperative sensing [13] is adopted and a base station will collect sensing information from mobile SUs to analyze and predict channel states. Besides, it is challenging to continuously sense PUs' status due to the mobility of SUs. To accommodate a mobile CRN, we improve H^2BMM, termed Advanced H^2BMM, by considering the discontinuous sensing behaviors of mobile SUs, .

Our main contributions are briefly summarized as below:

- For a stationary CRN, a novel High-order Hidden Bivariate Markov Model (H^2BMM) based spectrum prediction approach is proposed to fully inherit the strengths of high-order HMM and HBMM. In this approach, the prediction accuracy is enhanced by considering a underlying process and observing multiple previous states as well.

- Theoretical analysis is tailored to the training and prediction process for H^2BMM. The dimensionality of transition probability matrix in a standard HBMM is two. In H^2BMM, we increase the dimensionality so that one state depends on previous $m(m \geq 2)$ states. Accordingly, analysis of forward and backward possibilities is revised to calculate the conditional probability of the current state under its previous m and future m states.

- For a mobile CRN, we further improve the training algorithm of H^2BMM to adapt to the discontinuous sensing behaviors of mobile SUs because H^2BMM is originally developed when both PUs and SUs are fixed. The new training method of Advanced H^2BMM can achieve remarkably higher prediction accuracy in a mobile environment.

The rest of the paper is organized as follows. Related work on spectrum prediction is introduced in Section 2. Section 3 presents the detailed description of the proposed H^2BMM based spectrum prediction approach, along with theoretical analysis. Section 4 introduce the Advanced H^2BMM for a mobile environment. Simulation results are described in Section 5 and conclusions are drawn in Section 6.

2. Related Work

The growing concern over the spectrum scarcity has inspired considerable research on spectrum prediction in CRNs. Spectrum prediction is a necessary mean to address the spectrum fluctuation problem. Several common spectrum prediction algorithms, including HMM, HBMM and high-order HMM, are first introduced in this section, followed by a comparison among these solutions.

2.1. Hidden Markov Model (HMM) Based Prediction

In CRNs, the two-state channel model is commonly used, in which "0" and "1" indicate the channel being *idle* and *busy*, respectively. Since the actual channel state is typically hidden from SUs in HMM [8] [14], let $X = \{\text{“0”}, \text{“1”}\}$ denotes the actual and hidden state space, while $Y = \{\text{“0”}, \text{“1”}\}$ denote the observation/sensing state space.

The model training process is to adjust each element value of state transition probability matrix $A = [a_{ij}], i, j \in X$ and emission probability matrix $B = [b_{ij}], i, j \in Y$ [15]. As shown in Fig. 1, each element a_{ij} of state transition probability matrix A denotes the probability that the hidden channel state transfers from state "i" to state "j", while each element b_{ij} of emission probability matrix denotes the probability that hidden channel state "i" is observed as state "j" [16]. With the trained matrices and observation history, we are able to calculate the mostly likely hidden states chain and future states. In [17], HMM is applied to diagnose electronic circuit fault using high-order spectral analysis, but the high-order concept is different from that in our paper.

2.2. Hidden Bivariate Markov Model

HBMM can be viewed as an extension of standard HMM [18]. The main advantage of HBMM [10] [14] is that the dwell time in a given state has a discrete phase-type distribution which is more suitable for modeling a cognitive radio channel than the geometric dwell time distribution of HMM. In HBMM, each channel state contains r sub-states denoted by $\{S_n\}$. Let $\{Z_n = (X_n, S_n), n = 0, 1, \dots\}$ denote a discrete-time bivariate

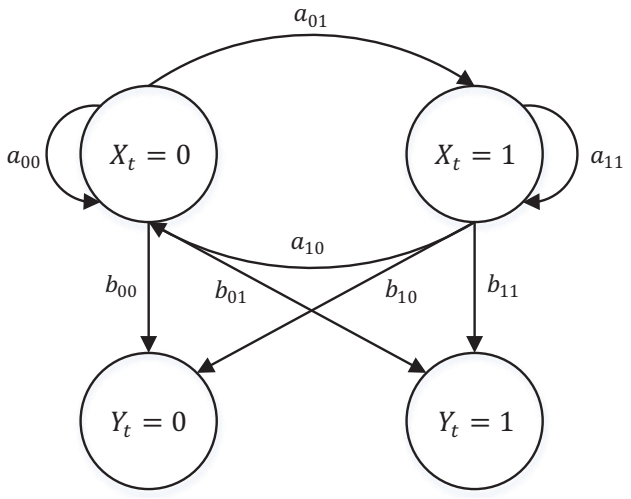

Figure 1. Hidden Markov Model (HMM) [14]

Markov chain. $\{X_n\}$ is referred to as the state process, while $\{S_n\}$ is the underlying process. The observable process denoted by $\{Y_n\}$ is obtained by observing the state process $\{X_n\}$ through a Gaussian memoryless channel. The transition matrix can be expressed by:

$$G = \begin{bmatrix} G_{11} & G_{12} \\ G_{21} & G_{22} \end{bmatrix}, \quad (1)$$

where $G_{ab} = \{g_{ab}(ij), i, j = 1, 2, \ldots, r\}$ is an $r \times r$ matrix.

2.3. High-order HMM

In the conventional first-order HMM, the prediction of current state is solely determined by its immediate previous state. High-order HMM [9] [14], instead, make predictions by considering multiple previous states [19]. As a result, first-order HMM and high-order HMM possess different transition matrix. Taking 2nd-order HMM [20] as an example, the size of transition matrix G is $n \times n \times n$ and each element g_{ijk} means the probability that the hidden channel state transfers from state "i" to state "j" and then to state "k". In general, when the order of high-order HMM increases, the performance is much better than the traditional HMM [21].

In summary, these typical prediction techniques have their advantages and disadvantages. There are two key problems of HMM. One is that the geometric dwell time distribution characteristic of the HMM is not adequate for modeling a cognitive radio channel, especially when bursty transmissions happen. Another one is that HMM is not able to fully explore the hidden correlation among adjacent observations because a state only depends on its previous one state. HBMM can be viewed as a modified HMM with better dwell time distribution characteristic through extending each hidden state to several sub-states. High-order HMM solves the limitation of low correlations and can obtain a better performance. Therefore, we combine the concept of High-order HMM and HBMM, and then propose a H^{2}BMM based spectrum prediction approach.

3. H^{2}BMM Based Spectrum Prediction

In this section, the proposed H^{2}BMM based spectrum prediction will be introduced. Before we delve into the details, the scenario of prediction on spectrum sensing is described first. We assume that the channel state alternates between "0 (*idle*)" and "1 (*busy*)". An SU observes the received signal and makes a sensing decision for the channel state: either "0 (*idle*)" or "1 (*busy*)". Taking energy detection as an instance, if the received energy amplitude exceeds a predefined threshold, the channel is perceived *busy*, otherwise the channel is determined as *idle*.

3.1. H^{2}BMM Parameters

Due to signal noise and interference, the sensed channel state does not necessarily represent the actual state. Therefore, we can view that the actual channel state is hidden from the SU. Let $X = \{$"0", "1"$\}$ denotes the hidden state space, with "0" and "1" indicating that the channel is idle and busy, respectively. Similarly, let $Y = \{$"0", "1"$\}$ denote the observation state space, with "0" and "1" indicating that the spectrum sensing results is idle and busy respectively. The principle of spectrum prediction is to predict future channel states from the historical channel states.

In terms of notation, capital letters are used to denote random variables and lower case letters to denote their realizations. Let $\{X_n\}$, $\{Y_n\}$ and $\{S_n\}$ represent the hidden process (i.e., the actual channel states), observation process (i.e., sensing results of channel state) and underlying process. Note that the underlying process $\{S_n\}$ takes values in $S = \{1, 2, \ldots, 5\}$, which implies that each channel state in X, *idle* ("0") or *busy* ("1"), contains 5 sub-states. The role of the underlying process $\{S_n\}$ is to facilitate mathematical analysis, i.e., induce a phase-type distribution on the dwell times of $\{X_n\}$ in the *idle* or *busy* state. Let $\{Z_n = (X_n, S_n), n = 0, 1, \ldots, N\}$ denotes the discrete-time bivariate Markov chain.

We assume that energy detection is employed for spectrum sensing and when channel state is *idle*, the observed signal strength $\{Y_n\}$ follows a Gaussian distribution with μ_0 mean and σ_0^2 variance. Similarly, when channel state is *busy*, $\{Y_n\}$ follows a Gaussian distribution with μ_1 mean and σ_1^2 variance.

The H^{2}BMM parameters, denoted by $\phi = (\pi, G, \mu, R)$, consist of an initial probability distribution π, a transition matrix G, a vector of mean observed signal strengths $\mu = \{\mu_0, \mu_1\}$, and a vector of observed signal strengths variances $R = \{\sigma_0^2, \sigma_1^2\}$. The size of transition matrix G is related with the order of H^{2}BMM. For

example, the size of G is $n \times n \times n$ for 2nd-order H^{2}BMM and each element g_{ijk} means the probability that the channel state transfers from state "i" to state "j" and then to state "k".

To better understand the concept of H^{2}BMM, we illustrate the 2nd-order H^{2}BMM with two sub-states in Fig. 2. As can be seen, each main state contains two sub-states and state transitions occur among these total four sub-states. Since this is for the 2nd-order model, the current state is related to its previous two states, i.e., from slot $n-2$ to $n-1$ and then to n.

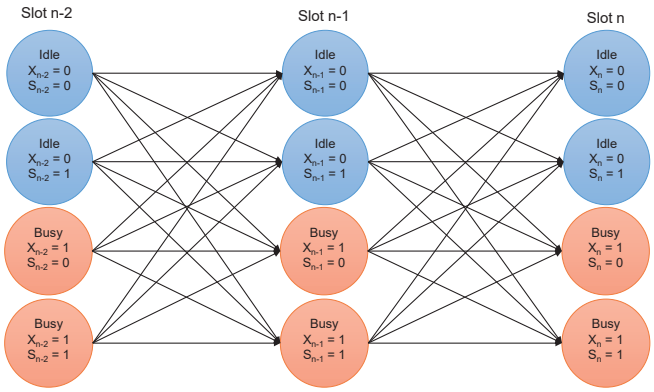

Figure 2. HHBMM Concept

3.2. H^{2}BMM

In this subsection, the proposed H^{2}BMM prediction procedures will be described in detail. Specifically, three major steps are involved. The first step is to generate a hidden channel state chain and observation chain as well. Then a training process is required for H^{2}BMM, in which the widely used Baum-Welch algorithm [22] is adopted. Last, the strategy of making a prediction decision is introduced. The following will detail each main step.

1) Generating hidden state chain and observation chain

For the channel states, we include the duration time for each state. It is assumed that the duration/dwell time of channel *busy* and *idle* states follows an exponential distribution, which is a special case of Phase distribution. That is, we consider the channel activity as a two-state model which incorporates *busy* and *idle* durations. The exponential distribution is used to generate a predictable hidden state chain $\{X_n, n = 0, 1, \ldots, 2N\}$,

$$f_B(x, \mu_B) = \begin{cases} \mu_B e^{-\mu_B x} & x \geq 0 \\ 0 & x < 0 \end{cases} \tag{2}$$

$$f_I(x, \mu_I) = \begin{cases} \mu_I e^{-\mu_I x} & x \geq 0 \\ 0 & x < 0 \end{cases} \tag{3}$$

where μ_B and μ_I are *busy* and *idle* duration parameters.

The channel duration distribution functions determine how long (i.e., how many time slots) the channel will remain in the current state. It is known the dwell/duration time of a channel state can be any positive value. Here we are interested in the channel state remaining for one time slot. Therefore, a new term is introduced called *transient state probability* to indicate the probability of channel state (*idle* or *busy*) remaining *for only one time slot*. The transient state probability significantly affects the performance of spectrum prediction, which will be evaluated in Section 5. We use transient state probability $P_{B\to I}$ to represent the probability of channel staying on *busy* for only one time slot. Similarly, $P_{I\to B}$ indicates the probability of *idle* state for one time slot. For example, in the case of $P_{B\to I} = 0.5$ and $P_{I\to B} = 0.8$, the possibility of one-slot dwell time in *busy* state is 50%, and the probability of one-slot dwell time in *idle* state is 80%. In other words, observing three consecutive time slots, if the current slot is *busy*, previous and next slots are both *idle*, this (i.e., staying in *busy* for only one time slot) occurs with a probability of 50%. If the current slot is *idle*, previous slot is *busy* and the next slot changes to *busy*, the likelihood of this (i.e., staying in *idle* for only one time slot) happening is 80%.

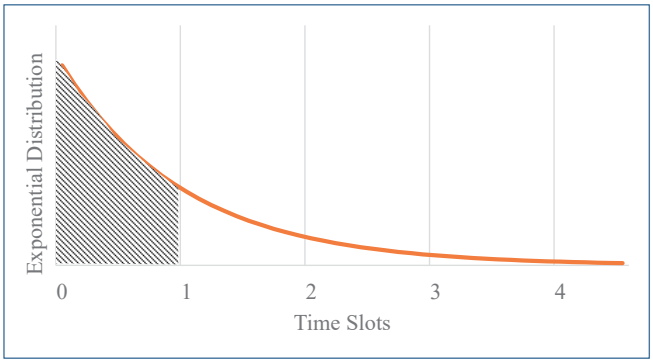

Figure 3. Illustration of calculating the transient state probability from an exponential duration distribution of a channel state

Fig. 3 illustrates an exponential duration/dwell distribution of a channel state. Since the transient state probability is defined as the probability of staying on the current state for one time slot, it is actually the integral of channel duration distribution functions from 0 to 1 (time slot), i.e., the shaded area in Fig. 3.

As a result, the formulas of $P_{B\to I}$ and $P_{I\to B}$ can be derived as below:

$$P_{B\to I} = \int_0^1 f_B(x, \mu_B)\, dx \tag{4}$$

$$P_{I\to B} = \int_0^1 f_I(x, \mu_I)\, dx \tag{5}$$

In addition, a signal strength observation chain $\{Y_n, n = 0, 1, \ldots, 2N\}$ is generated by applying Gaussian distribution. As mentioned previously, $\{Y_n\}$ follows a Gaussian distribution $N(\mu_0, \sigma_0^2)$ when $\{X_n\}$ is *idle*, and $\{Y_n\}$ follows a Gaussian distribution $N(\mu_1, \sigma_1^2)$ when $\{X_n\}$ is active.

2. H^2BMM Training

After generating the training sequence, H^2BMM is trained using the generated sequence. The widely used training algorithm of HMM is Baum-Welch algorithm. Based on the Baum-Welch algorithm, we design the training and prediction algorithm for H^2BMM. The m order HBMM training flow is summarized in Fig. 4. Once a new piece is received, the oldest piece will be abandoned. Given an initial parameter estimate $\phi = (\pi, G, \mu, R)$ and a piece of signal strength observations $\{Y_n, n = 0, 1, \ldots, N\}$, a parameter estimate $\hat{\phi} = (\hat{\pi}, \hat{G}, \hat{\mu}, \hat{R})$ with a higher likelihood is computed. Forward and backward probabilities are critical to estimate the parameter $\phi = (\pi, G, \mu, R)$, which will be factored in Eq. 9. After a certain number of iterations, a more accurate parameter estimate will be obtained.

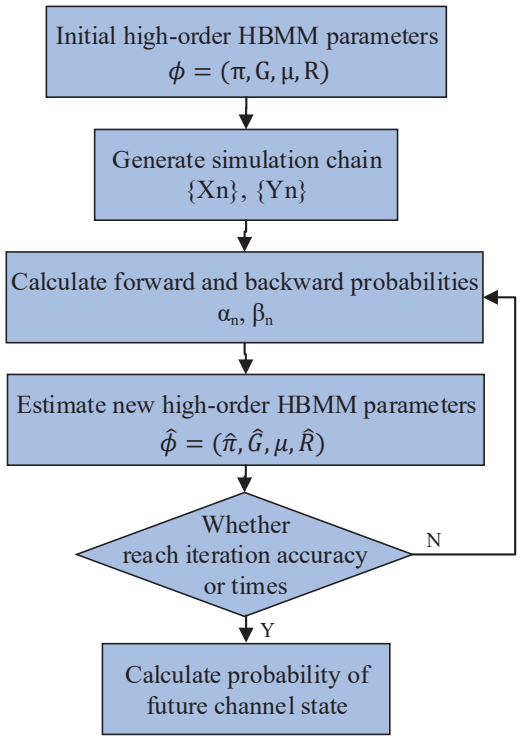

Figure 4. High-Order HBMM (H^2BMM) training flow

- Forward Probability

We define a forward probability, $\alpha_{kr}(n), k \in X, r \in S$, as the probability of current state $Z_n = \{X_n, S_n\}$ being (k, r) under the condition of previous n vectors $\{y_0, \ldots, y_{n-1}\}$. Define a 10×10 block diagonal matrix B_n, with its diagonal blocks given by $\{p(y_n|X_n = k)I, k \in X\}$. I is a 5×5 identity matrix. In Eq. 6, $\alpha(n)$ denotes a 1×10 vector of $\{\alpha_{01}(n), \ldots, \alpha_{05}(n), \alpha_{11}(n), \ldots, \alpha_{15}(n)\}$.

$$\begin{gathered}\alpha(0) = \pi B_0; \\ \cdots \\ \alpha(m-1) = \alpha(m-2)GB_{m-1}; \\ \cdots \\ \alpha(n) = \left[\left(\prod_{i=1}^{m} \alpha(n-i)\right) G\right] B_n,\ n = m, \ldots, N.\end{gathered} \tag{6}$$

where π denotes the initial states probability distribution and m denotes the order of H^2BMM. The recursive calculation of forward probability uses previous m forward probability. Therefore, we first calculate the forward probability of first m states: $\alpha(0)$ to $\alpha(m-1)$, from which $\alpha(m)$ can be determined. By repeating the process, with the forward probability of previous m states, forward probability of the following state, $\alpha(n), n = m+1, \ldots, N$, can be obtained.

- Backward Probability

Similarly, we define a backward probability, $\beta_{kr}(n), k \in X, r \in S$ as the probability of current state Z_n being (k, r) under the vectors of $\{y_{n+1}, \ldots, y_N\}$. In Eq. 7, $\beta(n)$ denotes a 1×10 vector of $\{\beta_{01}(n), \ldots, \beta_{05}(n), \beta_{11}(n), \ldots, \beta_{15}(n)\}$.

$$\begin{gathered}\beta(N) = \mathbf{1}' \\ \cdots \\ \beta(N-m+1) = \beta(N-m+2)B_{N-m+2}G'; \\ \cdots \\ \beta(n) = \left[\left(\prod_{i=m}^{1} \beta(n+i)\right) B_{n+1}\right] G', \\ n = N-m, \ldots, 0.\end{gathered} \tag{7}$$

where "′" denotes matrix transpose and "**1**" denotes a column vector of all ones. We calculate the backward probability of last m states: $\beta(N)$ to $\beta(N-m+1)$. With the backward probability of last m states, backward probability of the previous one state, $\beta(n)$, can be determined.

- Parameter Estimation

Applying the forward probability and backward probability formulas above, we can calculate the conditional probability $p(z_{n-m}, \ldots, z_{n-1}, z_n | y_0^N; \phi), n = 2, \ldots, N$ for H^2BMM in Eq. 8.

$$p(z_{n-m}, \ldots, z_{n-1}, z_n | y_0^N; \phi) = \frac{G(z_{n-m}, \ldots, z_{n-1}, z_n)Q(n)}{\sum_{z_{n-m}, \ldots, z_{n-1}, z_n} G(z_{n-m}, \ldots, z_{n-1}, z_n)Q(n)}, \tag{8}$$

where $Q(n) = \alpha(n-2)\beta(n)p(y_n|x_n)$.

The left side of this formula means the probability of $m+1$ states, $z_{n-m}, ..., z_{n-1}, z_n$, appearing in the whole observation sequence $\{Y_n\}$. The whole training computation complexity rises exponentially along with the increase of order index m, which leads to high computation delay. Taking both performance and complexity into consideration, we choose the order index to be two. In 2nd-order H^{2}BMM, current channel state depends on previous two states. Then we can regenerate the transition matrix G:

$$\hat{g}_{abc}(ijk) = \frac{\sum_{n=2}^{N} p(z_{n-2}=(a,i), z_{n-1}=(b,j), z_n=(c,k)|y_0^N;\phi)}{\sum_{(c,k)\in Z}\sum_{n=2}^{N} p(z_{n-2}=(a,i), z_{n-1}=(b,j), z_n=(c,k)|y_0^N;\phi)} \tag{9}$$

where $\hat{g}_{abc}(ijk)$ indicates the possibility of transferring from $z_{n-2}=(a,i)$ to $z_{n-1}=(b,j)$ and then to $z_n=(c,k)$.

In a standard HBMM, one state only depends on its previous one state. Each element of transition matrix of HBMM, $G(Z_{n-1}, Z_n)$, means the possibility of transferring from Z_{n-1} to Z_n. In our proposed H^{2}BMM, one state depends on previous two states. We redesign the training algorithm to generate a transition matrix with 3 dimensionalities. Each element of this 3D transition matrix, $G(Z_{n-2}, Z_{n-1}, Z_n)$, means the possibility of transferring from Z_{n-2}, Z_{n-1} to Z_n. The same as HMM, mean signal strengths vector μ and signal strengths variances vector R are also updated in each iteration. The variation of interferences throughout the simulation can reflect on μ and R because prediction model should be updated during the whole simulation period not just the initial training process.

3. Prediction Decision

Given the observation chain $\{Y_t\}$, a most likely $\{Z_t\}$ can be calculated. If the last two states of $\{Z_t\}$ are z_{n-1} and z_n, then the possibility of next state being z_{n+1} is $G(z_{n-1}, z_n, z_{n+1})$. Any possible z_{n+1} has its corresponding possibility. As we know, in a 2D matrix, if we specify the first one dimensionality, a vector can be selected. Similarly, in a 3D matrix, if we specify the first two dimensionalities, a vector can also be selected. Then the next state probability distribution can be expressed by

$$P(Z_{n+1}) = G(Z_{n-1}, Z_n, :) \tag{10}$$

where ":" denotes any possible z_n. Therefore, $P(Z_{n+1})$ is a vector where each element indicates the probability of a possible z_{n+1}.

Since channel state is either *idle* or *busy* and each state has 5 sub-states, $P(Z_{n+1})$ is a vector with length of 10. The first 5 elements of $P(Z_{n+1})$ mean the 5 sub-states of *idle* and the last 5 elements of $P(Z_{n+1})$ mean the 5 sub-states of *busy*. To determine the most possible z_{n+1}, we should find the maximum value of $P(Z_{n+1})$. If the order number of the maximum element in $P(Z_{n+1})$ is s, the next channel state X_{n+1} is

$$X_{n+1} = \begin{cases} 0 & s \le 5 \\ 1 & s > 5 \end{cases} \tag{11}$$

If the maximum value of $P(Z_{n+1})$ is located inside the first 5 elements, next one channel state X_{n+1} should be *idle*, otherwise X_{n+1} should be *busy*.

Multi-step prediction can be conducted the same as 1-step prediction. After we predict the next one channel state $\{X_{n+1}\}$, the previous $n+1$ channel states are viewed as historical data. Then the next two channel $\{X_{n+2}\}$ can be predicted.

4. Advanced H^{2}BMM Based Spectrum Prediction

As presented in Section 3.2, the H^{2}BMM is designed for stationary SUs to conduct spectrum prediction. In this section, a mobile CRN is considered and an extension of H^{2}BMM, named Advanced H^{2}BMM, is proposed.

4.1. Scenario

In a mobile CRN, SUs sense channel statuses and report sensing results to a Control Base Station (CBS) during their movement. The CBS is responsible for predicting the channel status. When an SU is moving towards a PU, at first, PU is out of the sensible range of SU, i.e., SUs can not sense the PU's existence. Hence, SUs determine that channel is in the *idle* state in this situation. After entering the sensible region of PU, SUs are able to sense the channel status.

The Advanced H^{2}BMM is applied to analyze historical sensing information and then predict future channel status. If the next channel state is predicted to be busy, SUs should exit the current channel in advance. After the channel is predicted to remain *idle* state, SUs can remain communications.

4.2. Advanced Training Algorithm

Due to the mobility of SUs, continuous sensing of any channel cannot be guaranteed. It should be noted that, in mobile CRNs, we can not guarantee continuous sensing data after taking user mobility into consideration. Therefore, the actual condition could be discontinuous sensing and the CBS may receive many

pieces of sensing data. In order to keep prediction matrix adapted to latest spectrum environment, we set TH_{tpn} as the threshold of training piece number. Therefore, instead of a whole sensing sequence $\{Y_n\}$, a CBS is likely to receive many sensing pieces as shown in Eq. 12.

$$\begin{array}{c} piece\ 1 : Y_{n1} = \{y_1, y_2, \ldots, y_i\} \\ piece\ 2 : Y_{n2} = \{y_1, y_2, \ldots, y_j\} \\ \ldots \\ piece\ m : Y_{nm} = \{y_1, y_2, \ldots, y_k\} \end{array} \tag{12}$$

where Y_{nm} indicates m^{th} sensing piece received by CBS. The length of received sensing pieces is random and there is no relationship between piece number and piece length. Piece length is random and could be any integer from 1 to simulation length. The training algorithm of the Advanced H^{2}BMM is revised by utilizing pieces of sensing sequences to update the training matrix, based on Subsection 3.2. The improvements are described as below.

- Forward Probability

In the Advanced H^{2}BMM, the forward possibility is calculated for each piece of sensing, which is denoted by $\alpha(n)_{piece\,i}$. Then the forward recursion is updated as below, based on Eq. 6 in subsection 3.2:

$$\begin{array}{c} \alpha(0)_{piece\,i} = \pi B_0; \\ \ldots \\ \alpha(m-1)_{piece\,i} = \alpha(m-2)_{piece\,i} G B_{m-1}; \\ \ldots \\ \alpha(n)_{piece\,i} = \left[\left(\prod_{i=1}^{m} \alpha(n-i)_{piece\,i} \right) G \right] B_n,\ n = m, \ldots, N. \end{array} \tag{13}$$

- Backward Probability

Similarly, the backward possibility for each piece of sensing, denoted by the $\beta(n)_{piece\,i}$, is derived based on Eq. 7 in subsection 3.2, as follows:

$$\begin{array}{c} \beta(N)_{piece\,i} = \mathbf{1}' \\ \ldots \\ \beta(N-m+1)_{piece\,i} = \beta(N-m+2)_{piece\,i} B_{N-m+2} G'; \\ \ldots \\ \beta(n)_{piece\,i} = \left[\left(\prod_{i=m}^{1} \beta(n+i)_{piece\,i} \right) B_{n+1} \right] G', \\ n = N-m, \ldots, 0. \end{array} \tag{14}$$

- Parameter Estimation

So far we have calculated the forward and backward possibilities for each sensing piece. By considering all pieces, the conditional probability is calculated in Eq. 15, which is revised based on Eq. 8 in subsection 3.2.

$$p(z_{n-m}, ..., z_{n-1}, z_n | y_0^N; \phi) = \frac{\sum_{all\ pieces} G(z_{n-m}, ..., z_{n-1}, z_n) Q(n)}{\sum_{all\ pieces} \sum_{z_{n-m}, ..., z_{n-1}, z_n} G(z_{n-m}, ..., z_{n-1}, z_n) Q(n)}, \tag{15}$$

5. Simulation Results

In this section, the performance of H^{2}BMM and Advanced H^{2}BMM are evaluated. First, H^{2}BMM is compared with two traditional models in a stationary CRN environment. For a mobile CRN environment, the Advanced H^{2}BMM is compared with H^{2}BMM to verify its advantages.

5.1. H^{2}BMM in Stationary CRNs

The proposed H^{2}BMM is evaluated in comparison with HMM and HBMM under a stationary environment, where both PUs and SUs are fixed. There are three key factors which affect the spectrum prediction performance of H^{2}BMM, i.e., transient state probability, prediction steps and order of H^{2}BMM. We evaluate the corresponding impact on the prediction performance by adjusting these factors.

First, prediction accuracies affected by the transient state probability are evaluated. As presented in Section 3, transient state probability $P_{B\to I}$ and $P_{I\to B}$ are calculated in Eqs. (4) and (5). The values of $P_{B\to I}$ and $P_{I\to B}$ can be altered by adjusting parameters of μ_B and μ_I, to simulate a various spectrum environment. Specifically, $P_{B\to I}$ is fixed to 0.8 while $P_{I\to B}$ is increased from 0.1 to 0.9, correspondingly μ_B is fixed to 1.61 while μ_I is increased from 0.11 to 2.30. We compare the prediction accuracy of H^{2}BMM, HBMM and HMM with 1-step prediction. Results are shown in Fig. 5.

Comparing these three lines in Fig 5, they have a similar V-shaped trend but H^{2}BMM obtains higher prediction accuracy than HMM and HBMM. From the line of 1-step HBMM in Fig. 5, it can be seen that the prediction accuracy is a V-shaped graph, starting considerably high around 87% when $P_{I\to B} = 0.1$, then it gradually decreases while $P_{I\to B}$ increases from 0.1 to 0.5. When $P_{I\to B} = 0.5$, the prediction accuracy reaches the lowest point. Afterwards, it continuously increases when $P_{I\to B}$ increases from 0.5 to 1. This trend is reasonable and can be interpreted as follows. When $P_{I\to B} = 0.1$, it means the probability of channel state experiencing *"busy-idle-busy"* for three consecutive slots is 0.1. That implies the probability that both the current and the next states are *idle* is 90%. In this situation, the spectrum has a strong pattern and thus future states are relatively easy to be predicted.

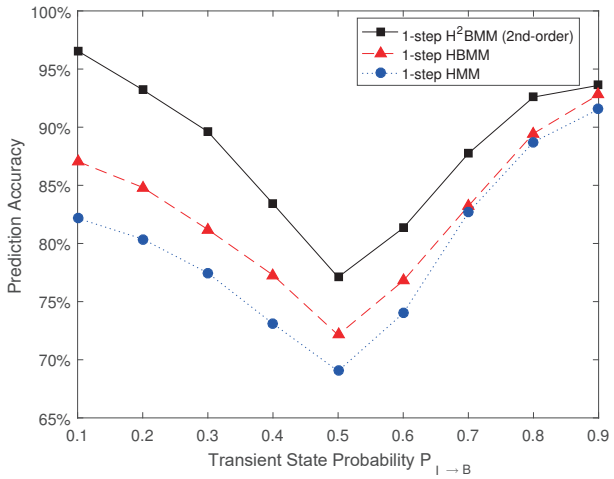

Figure 5. Prediction accuracy of H^{2}BMM, HBMM and HMM when $P_{B\to I} = 0.8$, $P_{I\to B}$ from 0.1 to 0.9

The prediction accuracy is lowest when the value of $P_{I\to B}$ is equal to 0.5. This is due to the fact when the transient state probability is close to 0.5, the possibility is approaching 50% for the next state to be *idle* or *busy*, which results in random and unpredictable spectrum pattern. Similarly, the spectrum pattern becomes stronger when $P_{I\to B}$ increases from 0.5 to 0.9. Consequently, the prediction accuracy keeps rising and achieves the highest point again when $P_{I\to B} = 0.9$.

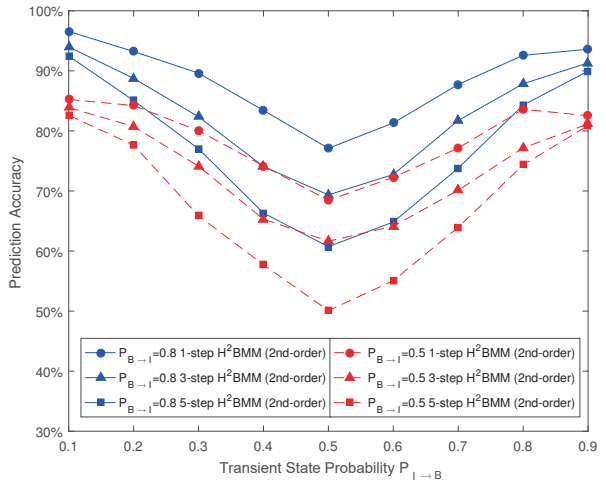

Figure 6. Prediction accuracy of H^{2}BMM (2nd-order) when $P_{B\to I}$ is 0.8 and 0.5

Second, the performance of 2nd-order H^{2}BMM is evaluated when $P_{B\to I}$ is set to 0.8 and 0.5, correspondingly μ_B is set to 1.61 and 0.69 respectively, while $P_{I\to B}$ increases from 0.1 to 0.9. The prediction accuracy of 1-step, 3-step and 5-step prediction are calculated, respectively. k-step prediction refers to that the channel states of next k slots instead of only one slot are predicted for each prediction. Results for 2nd-order H^{2}BMM are depicted in Fig 6.

In contrast, when the value of $P_{B\to I}$ is set to 0.5 and other factors are kept unchanged, all the prediction accuracies obtained by these three algorithms are relatively lower. Especially when the transient state probability reaches 0.5, the spectrum pattern becomes more and more random which greatly reduces the predict accuracy. However, the 1 step H^{2}BMM still achieves reasonable prediction accuracy even when the transient state probability reaches 0.5. In addition, the effect of prediction steps can also be observed from Fig. 6. The prediction of the 1-step achieves the highest accuracy, and the prediction accuracy decreases with the increase of steps.

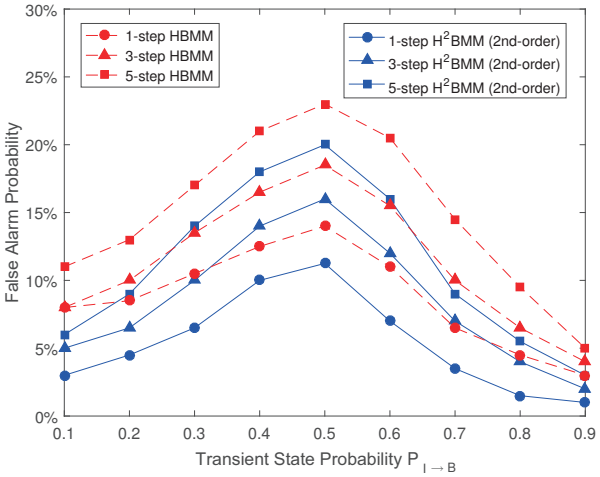

Figure 7. False alarm possibility of HBMM (1st-order) and H^{2}BMM (2nd-order)

Third, the false alarm and miss detection of the prediction achieved by the H^{2}BMM are evaluated. The false alarm probability means that the channel state is falsely detected as *busy* when the channel is actually *idle*, while miss detection is the opposite, that is, the channel state is false perceived as *idle* when the channel is actually *busy* [23]. In addition, order of H^{2}BMM indicates the correlation degree among adjacent observations. Higher order means the model can better explore the hidden correlation information from training sequences. In this simulation, we mainly compare the false alarm and miss detection achieved by the 1st-order H^{2}BMM, which becomes HBMM, and 2nd-order H^{2}BMM.

The probabilities of false alarm and miss detection for 1st-order H^{2}BMM (i.e., HBMM) and 2nd-order H^{2}BMM are depicted in Figs. 7 and 8, respectively. It can be seen that both the false alarm probability and miss detection probability of the prediction achieved by the H^{2}BMM

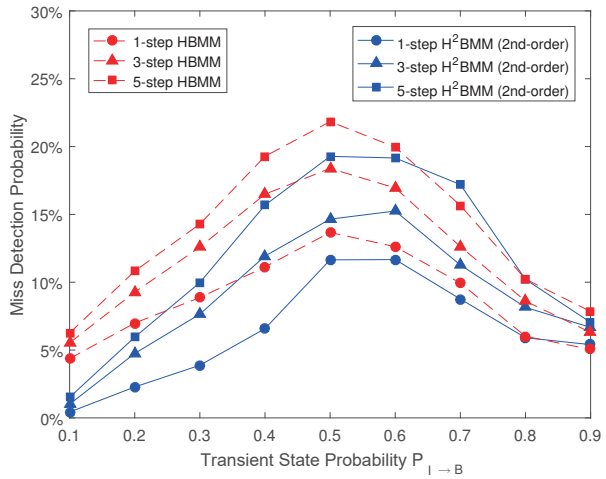

Figure 8. Miss detection possibility of HBMM (1st-order) and H^2BMM (2nd-order)

is obviously lower than that of the 1st-order H^2BMM (i.e., HBMM). In addition, the effect of multi-step can be observed. That is, higher-step leads to worse prediction accuracy for both 1st-order H^2BMM (i.e., HBMM) and 2nd-order H^2BMM.

Next, we evaluate the computation complexities between HMM, HBMM and H^2BMM by comparing the relative time consumed on performing the three algorithms. For a channel prediction algorithm, the computation complexity is proportional to three parameters, namely, the number of sub-states (r), the order index (m), and the prediction steps (k), which is verified in Fig. 9. As depicted in the figure, the 5-step H^2BMM has the highest time consumption, which is used as reference and set to be 100%. The consumed time reduces with the decrease of k, r and m. In addition, the order of of an algorithm has much heavier impact on the computation complexity than the prediction step. This could be observed by comparing the 1-steps H^2BMM and 1-step HBMM in Fig. 9. With the decrease of steps from 5 to 1, the time consumption of H^2BMM has slight degrade by 15%. By contrast, when changing the prediction algorithm from H^2BMM to HBMM, i.e., reducing the order of prediction algorithm from 2 to 1, the corresponding time consumption significantly drops from 86% to 43%.

In Fig. 10, we evaluate the average time consumption on spectrum discovery, which is referred to as the average interval for an SU to find an available channel. The spectrum prediction aims to accelerate the spectrum discovery process. If a channel is predicted to be *idle*, SUs will access the channel without sensing. Even if the predict results are wrong, it is acceptable as long as SUs exits the channel within the PU's tolerance period. If the channel is predicted as *busy*,

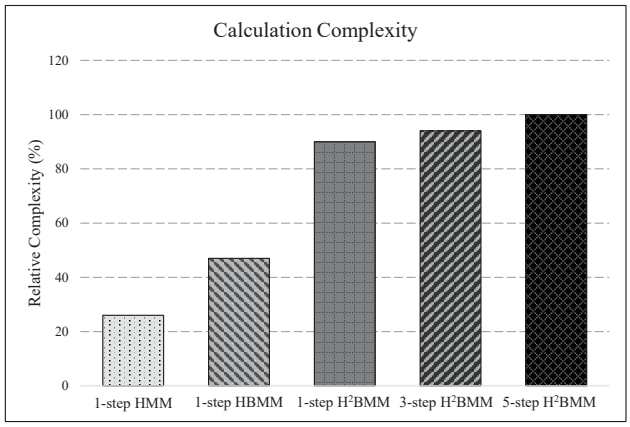

Figure 9. Computation Complexity of HMM, HBMM and H^2BMM

SUs will repeat the discovery process until an *idle* channel is found. As shown in the figure, H^2BMM spends less time than HMM and HBMM to discover an available channel. Besides, multi-step prediction can foresee the channel status of several future slots, which greatly reduces the time consumption of channel detection. Consequently, increasing the prediction steps of H^2BMM can further reduce the time consumption on spectrum discovery. In addition, through comparing Figs. 9 and 10, it reveals a trade-off between computation complexity and time consumption on spectrum discovery.

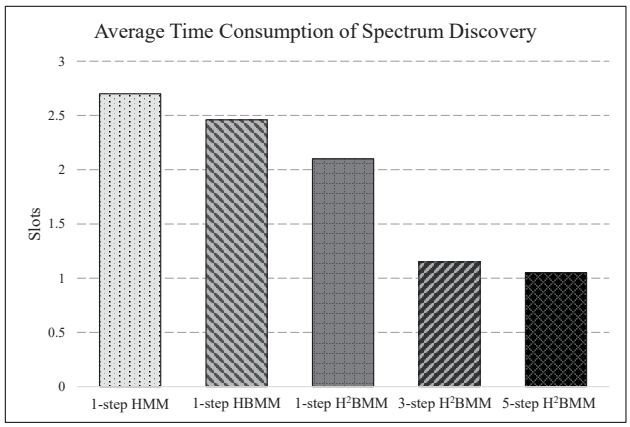

Figure 10. Time Consumption of HMM, HBMM and H^2BMM

5.2. Advanced H^2BMM vs. H^2BMM in a Mobile CRN

In this subsection, we compare the performance of the Advanced H^2BMM and H^2BMM in a mobile CRN. For both H^2BMM and Advanced H^2BMM, the cooperative sensing technique, i.e., majority fusion rule, is adopted to make a final decision. In contrast with the H^2BMM,

in which each SU detects the PU distributively and shares the sensing information with its neighbors, the Advanced H^{2}BMM collects the sensing data from SUs at the CBS for a centralized spectrum sensing.

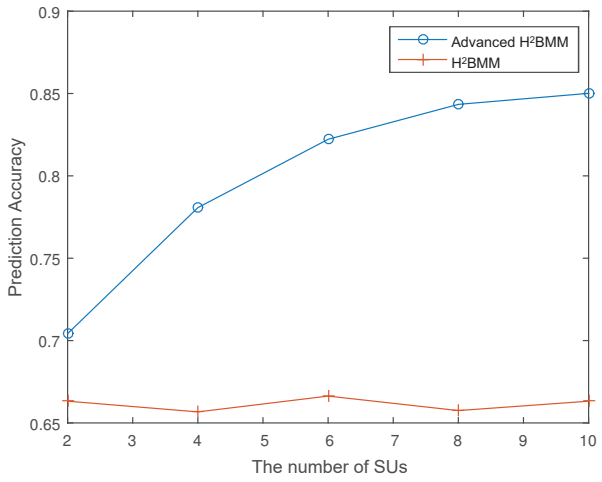

Figure 11. Prediction accuracy of Advanced H^{2}BMM and H^{2}BMM

We first evaluate the prediction accuracy of the Advanced H^{2}BMM and H^{2}BMM in Fig. 11. When a mobile SU moves into the protected area of a PU, both the Advanced H^{2}BMM and H^{2}BMM can update their training matrix based on the new sensing result so that the prediction model can adapt to the new spectrum environment timely. However, as demonstrated in Fig. 11, their prediction accuracies have significant difference. The Advanced H^{2}BMM achieves higher prediction accuracy than the H^{2}BMM benefiting from the centralized spectrum sensing on the CBS. The increased number of SUs sending the sensing data to CBS brings better training on the matrix of H^{2}BMM and improves the prediction accuracy, as illustrated in Fig. 11. By contrast, for H^{2}BMM, the increase of SU number has no evidential impact on the prediction accuracy since each SU conducts the spectrum sensing and prediction independently. The prediction accuracy of H^{2}BMM, therefore, is much lower than that of the advanced H^{2}BMM in a mobile CRN environment.

Fig. 12 compares the false alarm possibilities of H^{2}BMM and Advanced H^{2}BMM. As shown in the figure, when the number of SUs is less than three, the CBS of Advanced H^{2}BMM cannot collect sufficient sensing reports for an accurate channel prediction. Therefore, the Advanced H^{2}BMM has a higher false alarm possibility than H^{2}BMM when the number of SUs is less than 3. When more SUs join the network, the CBS in the Advanced H^{2}BMM collects more sensing information from SUs and becomes better aware of the surrounding channel behavior and hence reduces the

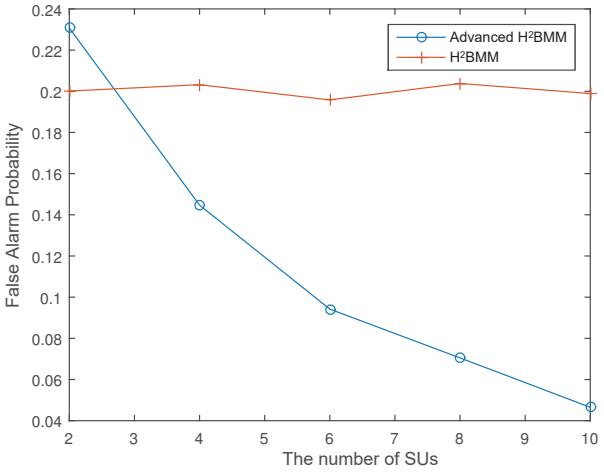

Figure 12. False alarm of Advanced H^{2}BMM and H^{2}BMM

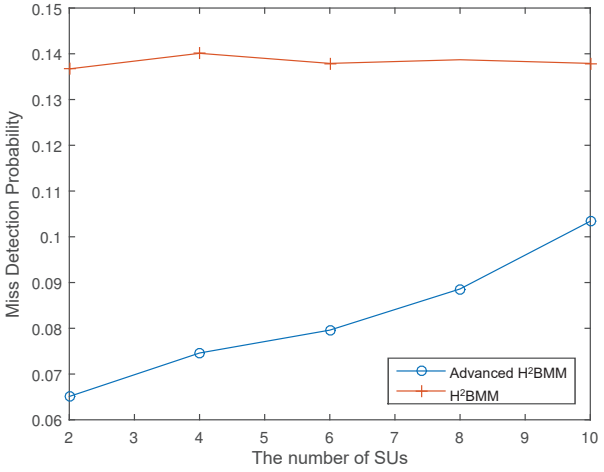

Figure 13. Miss detection of Advanced H^{2}BMM and H^{2}BMM

false alarm probability. The reason why the increase of SU number has no significant effect on H^{2}BMM has been explained in Fig. 11.

In Fig. 13, the miss detection probabilities of Advanced H^{2}BMM and H^{2}BMM are presented. As illustrated in the figure, the Advanced H^{2}BMM has a lower miss detection possibility than H^{2}BMM because the former obtains better training sequence and adopts an enhanced matrix training method. In Advanced H^{2}BMM, if the CBS cannot collect sufficient sensing information for an accurate spectrum prediction, it tends to set the status of the future channel as *busy*. Using such a conservative strategy, the SUs have a less chance to interfere with the PU; the opportunity that an SU access the channel, however, is also reduced. As illustrated in Fig. 13, the miss detection rate is as low as 0.65 when the number of SUs is less than 3. With the increase of the SU number, the CBS can obtain more

sensing data and hence to decrease prediction tendency of status *busy*. Similarly, the slight effect of the increase of SU numbers on H^{2}BMM has been explained in Fig. 11.

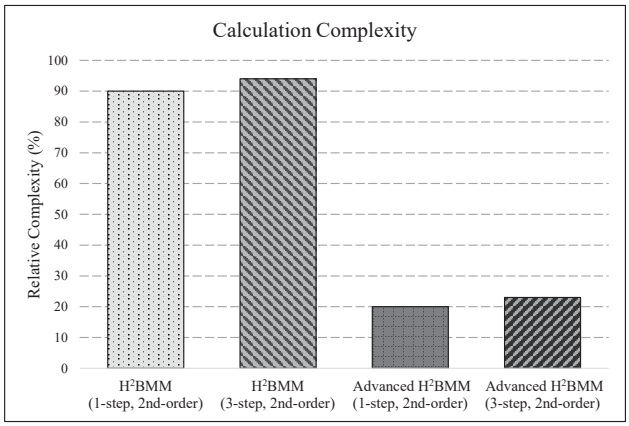

Figure 14. Computation Complexity of Advanced H^{2}BMM and H^{2}BMM

Now, we compare the computational complexities of Advanced H^{2}BMM and H^{2}BMM in a mobile CRN environment, and show the results in Fig. 14. As we discussed in Fig. 9, the computational complexity is proportional to three parameters, namely, r, m, and k. Therefore, a processor takes a longer time to perform an algorithm with more prediction steps. As observed in Fig. 14, the time consumption of 1-step H^{2}BMM is 90%, which is slightly lower than the 3-step H^{2}BMM. In addition, owing to the enhanced training method, the computational complexities of the 1-step and 3-step Advanced H^{2}BMM are 19% and 23%, respectively, which are much lower than that of the H^{2}BMM. Specifically, in the Advanced H^{2}BMM, the training method is improved so that the CBS only needs to calculate the forward and backward probabilities for a small portion of training sequences. By contrast, an SU in H^{2}BMM needs to calculate the forward and backward possibilities of the whole training sequence, which remarkably increases the computational complexity.

The time that H^{2}BMM and Advanced H^{2}BMM spent on discovering the vacant channel is illustrated in Fig. 15. Recall that Fig. 10 indicates less time consumption on spectrum discovery with increased prediction steps. For H^{2}BMM, the time consumptions of 1-step and 3-step prediction are 6.8 and 3.5 slots, respectively, which is accelerated to 2.3 and 1.2 slots in the 1-step and 3-step Advanced H^{2}BMM, respectively. Particularly, the Advanced H^{2}BMM is specially designed for a mobile CRN environment and the H^{2}BMM is initially designed for a stationary CRN.

To summarize, the Advanced H^{2}BMM has superior performance than H^{2}BMM in a mobile CRN, in terms

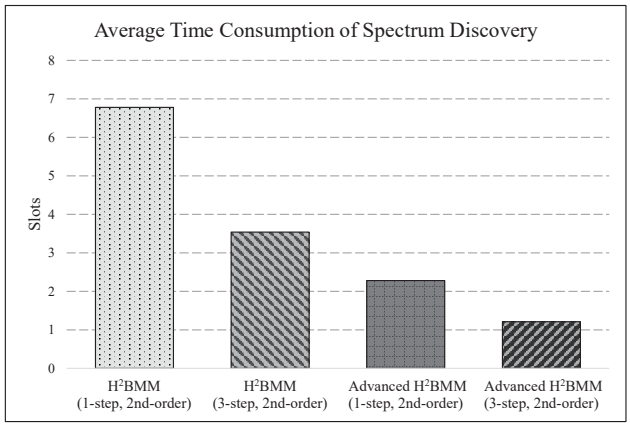

Figure 15. Time Consumption of Advanced H^{2}BMM and H^{2}BMM

of higher prediction accuracy, smaller false alarm and miss detection probabilities, lower computation complexity and less time consumption on spectrum discover.

6. Conclusion

In this paper, we have proposed a new spectrum prediction approach, called the H^{2}BMM for CRN. The proposed approach fully explores the hidden correlation of previous states to make a spectrum prediction. Therefore, it remarkably increases the prediction accuracy compared with the conventional spectrum prediction approaches. To achieve a satisfactory performance in a mobile CRN environment, an Advance H^{2}BMM algorithm is also designed through improving the training method of H^{2}BMM. Extensive simulations have been carried out and results verify that the prediction performance is significantly improved. The computational complexity and the time consumption for spectrum discovery are evaluated as well.

References

[1] R. Heydari, S. Alirezaee, S. V. Makki, M. Ahmadi, and S. Erfani, "Cognitive radio channel behavior prediction using the hidden Markov model," in *Proceedings of the 7th IEEE International Symposium on Telecommunications (IST)*, 2014, pp. 993–998.

[2] S. H. Sohn, S. J. Jang, and J. M. Kim, "HMM-based adaptive Frequency-hopping cognitive radio system to reduce interference time and to improve throughput," *KSII Transactions on Internet and Information Systems (TIIS)*, vol. 4, no. 4, pp. 475–490, 2010.

[3] Y. Song and J. Xie, "Prospect: A proactive spectrum handoff framework for cognitive radio ad hoc networks without common control channel," *IEEE Transactions on Mobile Computing*, vol. 11, no. 7, pp. 1127–1139, 2012.

[4] Z. Lin, X. Jiang, L. Huang, and Y. Yao, "A energy prediction based spectrum sensing approach for cognitive

radio networks," in *Proceedings of the 5th IEEE International Conference on Wireless Communications, Networking and Mobile Computing*, 2009, pp. 1–4.

[5] Y. Zhao, M. Song, C. Xin, and M. Wadhwa, "Spectrum sensing based on Three-State model to accomplish all-level fairness for Co-Existing multiple cognitive radio networks," in *Proceedings of the IEEE Conference on Computer Communications (INFOCOM)*, 2012, pp. 1782–1790.

[6] E. Ahmed, L. J. Yao, M. Shiraz, A. Gani, and S. Ali, "Fuzzy-based spectrum handoff and channel selection for cognitive radio networks," in *Proceedings of the IEEE International Conference on Computer, Control, Informatics and Its Applications (IC3INA)*, 2013, pp. 23–28.

[7] X. Xing, T. Jing, W. Cheng, Y. Huo, and X. Cheng, "Spectrum prediction in cognitive radio networks," *IEEE Transactions on Wireless Communications*, vol. 20, no. 2, pp. 90–96, 2013.

[8] A. M. Mikaeil, B. Guo, X. Bai, and Z. Wang, "Hidden Markov and Markov switching model for primary user channel state prediction in cognitive radio," in *Proceedings of the 2nd IEEE International Conference on Systems and Informatics (ICSAI)*, 2014, pp. 854–859.

[9] Z. Chen and R. C. Qiu, "Prediction of channel state for cognitive radio using Higher-order hidden Markov model," in *Proceedings of the IEEE SoutheastCon Conference (SECON)*, 2010, pp. 276–282.

[10] T. Nguyen, B. L. Mark, and Y. Ephraim, "Spectrum sensing using a hidden bivariate Markov model," *IEEE Transactions on Wireless Communications*, vol. 12, no. 9, pp. 4582–4591, 2013.

[11] S. Geirhofer, L. Tong, and B. M. Sadler, "Cognitive radios for dynamic spectrum Access-dynamic spectrum access in the time domain: Modeling and exploiting white space," *IEEE Communications Magazine*, vol. 45, no. 5, pp. 66–72, 2007.

[12] K. D. Singh, P. Rawat, and J.-M. Bonnin, "Cognitive radio for vehicular ad hoc networks (CR-VANETs): approaches and challenges," *EURASIP Journal on Wireless Communications and Networking*, vol. 2014, no. 1, p. 1, 2014.

[13] K. M. Thilina, K. W. Choi, N. Saquib, and E. Hossain, "Machine learning techniques for cooperative spectrum sensing in cognitive radio networks," *IEEE Journal on Selected areas in Communications*, vol. 31, no. 11, pp. 2209–2221, 2013.

[14] E. Chatziantoniou, B. Allen, and V. Velisavljevic, "An hmm-based spectrum occupancy predictor for energy efficient cognitive radio," in *Proceedings of the 24th IEEE International Symposium on Personal Indoor and Mobile Radio Communications (PIMRC)*, 2013, pp. 601–605.

[15] C. Chen, G. Vachtsevanos, and M. E. Orchard, "Machine remaining useful life prediction: An integrated adaptive Neuro-fuzzy and High-order particle filtering approach," *Elsevier Mechanical Systems and Signal Processing*, vol. 28, pp. 597–607, 2012.

[16] D. Treeumnuk and D. C. Popescu, "Using hidden Markov models to evaluate performance of cooperative spectrum sensing," *IET Communications*, vol. 7, no. 17, pp. 1969–1973, 2013.

[17] R. W. Yan, L. Zhou, and Z. Y. Zhong, "Application of algorithm of hidden Markov model and High-order spectrum in fault diagnosis of power electronic circuit," in *Advanced Materials Research*, vol. 468. Trans Tech Publ, 2012, pp. 488–491.

[18] B. L. Mark and Y. Ephraim, "An em algorithm for continuous-time bivariate Markov chains," *Elsevier Computational Statistics & Data Analysis*, vol. 57, no. 1, pp. 504–517, 2013.

[19] T. Black, B. Kerans, and A. Kerans, "Implementation of hidden Markov model spectrum prediction algorithm," in *Proceedings of the IEEE International Symposium on Communications and Information Technologies (ISCIT)*, 2012, pp. 280–283.

[20] J. Lan, X. R. Li, V. P. Jilkov, and C. Mu, "Second-order Markov chain based Multiple-model algorithm for maneuvering target tracking," *IEEE Transactions on Aerospace and Electronic Systems*, vol. 49, no. 1, pp. 3–19, 2013.

[21] W. Zhao, J. Wang, and H. Lu, "Combining forecasts of electricity consumption in China with TimeVarying weights updated by a High-Order Markov chain model," *Omega International Journal of Management Science*, vol. 45, pp. 80–91, 2014.

[22] L. R. Welch, "Hidden Markov models and the Baum-Welch algorithm," *IEEE Information Theory Society Newsletter*, vol. 53, no. 4, pp. 10–13, 2003.

[23] C. Pham, N. H. Tran, C. T. Do, S. I. Moon, and C. S. Hong, "Spectrum handoff model based on hidden Markov model in cognitive radio networks," in *Proceedings of the IEEE International Conference on Information Networking (ICOIN)*, 2014, pp. 406–411.